NJP317829 on 5 August 2009

New Journal of Physics
The open-access journal for physics

Heat conduction in graphene: experimental study and theoretical interpretation

S Ghosh, D L Nika[1], E P Pokatilov[1] and A A Balandin[2]

Nano-Device Laboratory, Department of Electrical Engineering and Materials Science and Engineering Program, University of California—Riverside, Riverside, CA 92521, USA
E-mail: balandin@ee.ucr.edu

New Journal of Physics **11** (2009) 000000 (18pp)
Received 8 May 2009
Published xxx
Online at http://www.njp.org/
doi:10.1088/1367-2630/11/8/000000

Abstract. We review the results of our experimental investigation of heat conduction in suspended graphene and offer a theoretical interpretation of its extremely high thermal conductivity. The direct measurements of thermal conductivity of graphene were performed using a non-contact optical technique and special calibration procedure with bulk graphite. The measured values were in the range of ~3000–5300 W mK^{-1} near room temperature and depended on the lateral dimensions of graphene flakes. We explain the enhanced thermal conductivity of graphene as compared to that of bulk graphite basal planes by the two-dimensional nature of heat conduction in graphene over the whole range of phonon frequencies. Our calculations show that the intrinsic Umklapp-limited thermal conductivity of graphene grows with the increasing dimensions of graphene flakes and can exceed that of bulk graphite when the flake size is on the order of a few micrometers. The detailed theory, which includes the phonon-mode-dependent Gruneisen parameter and takes into account phonon scattering on graphene edges and point defects, gives numerical results that are in excellent agreement with the measurements for suspended graphene. Superior thermal properties of graphene are beneficial for all proposed graphene device applications.

[1] On leave from the Department of Theoretical Physics, Moldova State University, Chisinau, Republic of Moldova.
[2] Author to whom any correspondence should be addressed.

Contents

1. Introduction

It was recently discovered experimentally that graphene [1, 2] has an extremely high thermal conductivity [3, 4]. The measurements reported by Balandin *et al* [3, 4] were performed using the non-contact optical technique, where the local temperature rise due to laser heating was determined through the independently measured temperature coefficients of the graphene Raman G peak [5, 6]. It was found that the near room-temperature (RT) thermal conductivity of partially suspended single-layer graphene is in the range $K \sim 3000$–$5300\,\mathrm{W\,mK^{-1}}$ depending on the graphene flake size. These experimental findings stimulated a body of theoretical work on the subject. Nika *et al* [7] performed a detailed numerical study of the lattice thermal conductivity of graphene using the phonon dispersion obtained by the valence-force field (VFF) method. The authors treated the three-phonon Umklapp scattering directly considering all phonon relaxation channels allowed by the energy and momentum conservation in the graphene two-dimensional (2D) Brillouin zone (BZ) [7]. Jiang *et al* [8] calculated the thermal conductance of graphene in the pure ballistic limit obtaining a high value, which translates to the thermal conductivity in excess of $\sim 6600\,\mathrm{W\,mK^{-1}}$. The higher thermal conductivity is expected for the ballistic regime when no scattering is included. Lan *et al* [9] determined the thermal conductivity of graphene nanoribbons by combining the tight-binding approach and the phonon non-equilibrium Green's function method. The authors found a thermal conductivity $K = 3410\,\mathrm{W\,mK^{-1}}$ [9], which is clearly above the bulk graphite limit of $2000\,\mathrm{W\,mK^{-1}}$ and in agreement with the first experiments [3, 4]. Strong edge and flake size effects were also revealed by the numerical data in line with the experiments [3, 4].

In this paper, we review our experimental results, provide details of the data extraction procedure and offer a physical interpretation of heat conduction in graphene. Our theoretical model allowed us to explain the higher values of thermal conductivity in suspended graphene as compared to that of basal planes of bulk graphite. The rest of the paper is organized as follows. Section 2 describes the method developed for measuring the thermal conductivity of the suspended graphene. In section 3, we provide details of the measurements and calibration procedure. Section 4 outlines the formal theory of the thermal conductivity. It is an accurate approach but very challenging computationally. In order to treat the three-phonon Umklapp processes exactly, we propose the scattering diagram method. In section 5, we offer a simple model of the thermal conductivity of graphene. This model is less accurate but allows one to clearly see the physical reasons behind higher thermal conductivity of graphene as compared to

that of basal planes of bulk graphite. It also explains the inherent importance of the lateral size effects on the thermal conductivity of graphene flakes.

2. Experimental investigation of heat conduction in graphene

Since none of the conventional methods for the thermal conductivity measurement works for graphene, we developed our own non-contact optical approach. We took advantage of the fact that graphene has distinctive signatures in Raman spectra with clear G peak and 2D band [10]–[13]. Moreover, we also found that the G peak of graphene's Raman spectra exhibits strong temperature dependence [5, 6]. The latter means that the shift in the position of G peak in response to laser heating can be used for measuring the local temperature rise. The correlation between the temperature rise and amount of power dissipated in graphene, for the sample with given geometry and proper heat sinks, can give the value of the thermal conductivity K (see the schematic of the experiment in figure 1(a)). Even a small amount of power dissipated in graphene can be sufficient for inducing a measurable shift in the G peak position due to the extremely small thickness of the material—one atomic layer. The suspended portion of graphene served several essential functions for (i) accurately determining the amount of power absorbed by graphene through the calibration procedure, (ii) forming 2D in-plane heat front propagating toward the heat sinks and (iii) reducing the thermal coupling to the substrate through the increased micro and nanoscale corrugations (see figure 1(b)).

The first step in the measurements was determining the temperature coefficient χ_G for the G peak. To accomplish this task the laser excitation power was kept at a minimal level and the temperature of the graphene flake was changed externally through the hot–cold cell [5, 6]. The results of our measurement of the temperature coefficients were verified by measuring the coefficients for bulk graphite, which were in excellent agreement with the previously published data for graphite [5, 6]. After the change in the temperature ΔT has been correlated with the change in the $\Delta\omega$ peak position, the micro-Raman spectrometer can be used as a thermometer. During the measurement of the thermal conductivity, the excitation power is intentionally increased to induce the local heating. The local temperature rise is determined through the expression $\Delta T = \Delta\omega_G/\chi_G$. It is important to mention here that the measurement technique is steady state. Each data point in the thermal conductivity measurement, i.e. in recording the G peak position as a function of the excitation power, takes sufficient time (several minutes) for achieving the steady state. The energy deposited by the laser light to the electron gas in graphene is transferred to phonons very fast. The time constant for the energy transfer from the electrons to acoustic phonons in graphene is on the order of several picoseconds [14]–[16]. Thus, for the large graphene flakes utilized in our experiments (tens of microns) the changes in the induced hot spot due to the finite thermalization time are small and can be neglected. From the other side, our measurement time was small compared to the hours, that are required in order to induce damage or surface modification in graphene by the laser light [17].

The long graphene flakes for these measurements were produced using the standard technique of mechanical exfoliation of bulk Kish and highly oriented pyrolytic graphite (HOPG) [1, 2]. The trenches were fabricated using the reactive ion etching. The width of these trenches ranged from 1 to 5 μm with the nominal depth of 300 nm. In the first set of measurements, we selected graphene flakes of approximately rectangular shape connected to large graphitic pieces, which acted as heat sinks. The rectangular shape was selected in order to use a simple data extraction procedure based on the 1D heat diffusion equation. These graphitic

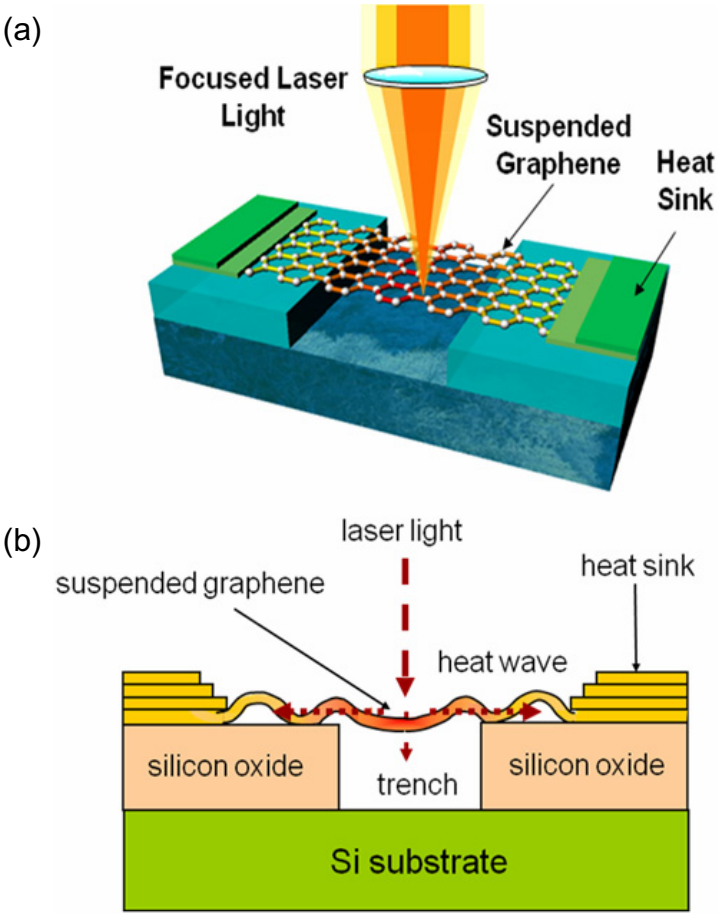

Figure 1. (a) Schematic of the experimental setup with the excitation laser light focused on graphene suspended across a trench in Si wafer. Laser power absorbed in graphene induces a local hot spot and generates heat wave propagating toward the heat sinks. (b) Illustration of the micro and nanoscale corrugation formed in the suspended flake, which further reduce the thermal coupling to the substrate. The depicted experimental technique allows one for the steady-state non-contact direct measurement of the thermal conductivity.

pieces were at a distance of a few micrometers from the trench edges to ensure that the transport is at least partially diffusive and the phonon mean free path (MFP) is not limited just by the length of the flake. In the later measurements, we utilized well-defined massive metal heat sinks and an elaborate procedure for the thermal conductivity extraction based on the numerical solution of the heat diffusion equation. The single-layer graphene flakes were selected using the micro Raman spectroscopy by checking the intensity ratio of G and 2D peaks and by 2D band deconvolution [10]–[13]. The combination of these two Raman techniques with the atomic force microscopy (AFM) and scanning electron microscopy (SEM) allowed us to verify the number of atomic planes and flake uniformity with a high degree of accuracy. The 2D band deconvolution is currently considered to be the most robust, non-destructive and accurate technique for counting the number of atomic layers in graphene. One should note here that the thermal interface resistance between the flake and the heat sink is not such a big issue like in

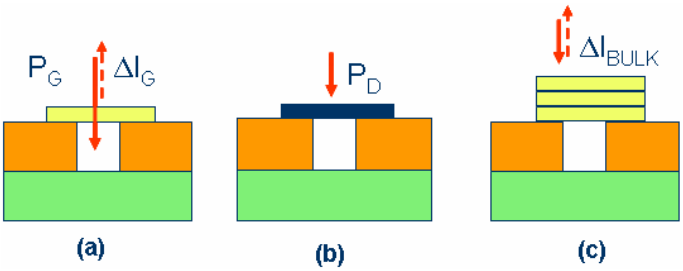

Figure 2. Illustration of the measurement and calibration procedure. (a) Integrated Raman intensity is related to the power absorbed in graphene through the scattering cross-section and absorption coefficient. (b) Detector is placed at the sample location to measure the power at the surface. (c) Bulk graphite is used as reference for the calibration procedure. The power absorbed in graphene is determined through the ratio of the integrated Raman intensities of graphene and bulk graphite.

the case of carbon nanotubes (CNTs). The graphene flake is naturally attached to the graphitic piece and heat spreads over a large area.

The challenge in the measurement of the thermal conductivity with the described optical technique is in accurate determining of the power absorbed in graphene. Only a fraction P_G of the laser light focused on the graphene flake will actually be dissipated in the graphene. Most of the light will be reflected back after the light travels through the flake to the trench bottom and is reflected back (see figures 1(a) and (b)). The power, which is measured by the detector placed at the position of the flake, is the total power P_D, part of which goes into the graphene flake after two transmissions (incident pass and reflected pass) and the rest is lost in the silicon wafer P_{Si}. It is now known that the fraction of the power absorbed by graphene is 2.3% per layer for light wavelength $\lambda > 500$ nm. Our measurements were performed at a smaller wavelength ($\lambda = 488$ nm) where the absorption is enhanced [18, 19]. The stronger absorption at smaller wavelengths is explained by the effect of surface contaminations and bending of the suspended part of graphene. The near-field effects in the gap between the suspended graphene and trench bottom may also lead to additional absorption. Thus, it was important to determine the absorbed power in the specific conditions of our experiment. The power P_G was measured through the calibration procedure with the bulk graphite serving as a reference. The calibration and measurement of the absorbed power is illustrated in figure 2. It is based on comparison of the experimentally determined integrated Raman intensity for the G peak from the single-layer graphene and bulk graphite. In the next section, we give the details of the derivation of the calibration formula for the single-layer graphene. The measurements over the trenches with different depths excluded interference effects [12]. No electrical bias was used at the back gate or heat sinks to avoid the electrostatic effects on the G peak position. The RT position of the G peak was verified for all samples.

3. Details of the measurements and data extraction technique

In this section, we provide details of the derivation of the formulae, which allow us to determine the fraction of light power absorbed in graphene. The intensity of Raman scattering in graphene

is given by

$$\Delta I_{\mathrm{G}} = N\sigma_{\mathrm{G}} I_0, \tag{1}$$

where N is the number of scattering atoms on the illuminated surface of the cross-section A, I_0 is the laser intensity and σ_{G} is the Raman scattering cross-section. Let us assume that an electromagnetic (EM) wave with the intensity $I = I_0$ is incident on a graphene layer. The electric field of the wave transmitted through the graphene layer can be written as $\vec{E}_1 = \vec{E}_0 \exp[2\pi\,\mathrm{i}(n_0 + \mathrm{i}\kappa)a_{\mathrm{G}}/\lambda - \mathrm{i}\omega t]$, where n_0 is the refractive index, κ the extinction index and a_{G} the graphene thickness. Using the notations $A_1 = 2\pi\kappa a_{\mathrm{G}}/\lambda$ and $A_2 = 2\pi n_0 a_{\mathrm{G}}/\lambda$, we can rewrite the above equation as $\vec{E}_1 = \vec{E}_0 \exp[-A_1]\exp[\mathrm{i}(A_2 - \omega t)]$. The power absorbed in the graphene monolayer is given by the expression

$$\begin{aligned} P_{G,1} &= A(I_0 - I_1) = A[\langle(\mathrm{Re}E_0)^2\rangle_t - \langle(\mathrm{Re}E_1)^2\rangle_t] \\ &= (1/2)AE_0^2(1 - \exp[-2A_1]) \approx 2A_1 A I_0 = \alpha_{\mathrm{G}} a_{\mathrm{G}} A I_0, \end{aligned} \tag{2}$$

where the averaging is carried over the wave period $T = 2\pi/\omega$ and $\alpha_{\mathrm{G}} = 4\pi\kappa/\lambda$. The EM wave incident on the surface of silicon under the suspended graphene is given as

$$\vec{E}_2 = \vec{E}_0 \exp[-A_1]\exp[\mathrm{i}(A_2 - \omega t + 2\pi z_0/\lambda)], \tag{3}$$

where z_0—is the distance from the graphene monolayer to the silicon surface (trench bottom), which gives an extra phase factor of $\exp[2\pi\,\mathrm{i}z_0/\lambda]$. The reflected wave from silicon will have a different amplitude $\vec{E}_{\mathrm{r}}$ and additional phase φ given as

$$\vec{E}_3 = \vec{E}_{\mathrm{r}} \exp[\mathrm{i}(A_2 - \omega t + 2\pi z_0/\lambda + \varphi)]. \tag{4}$$

By definition, the measurable macroscopic reflection coefficient is a ratio of the intensities of the incident and reflected waves, i.e. $R_{\mathrm{Si}} = I_3/I_2$. Here, we can write the following:

$$I_2 = (1/2)E_0^2 \exp[-2A_1] = I_0 \exp[-2A_1], \qquad I_3 = (1/2)E_{\mathrm{r}}^2. \tag{5}$$

Thus, the reflection coefficient can be expressed as: $R_{\mathrm{Si}} = E_{\mathrm{r}}^2/E_0^2 \exp[-2A_1]$, which gives the relationship: $E_{\mathrm{r}}^2 = R_{\mathrm{Si}} E_0^2 \exp[-2A_1]$. The amplitude of the reflected wave on the bottom side of the suspended graphene monolayer is given as

$$\vec{E}_4 = \vec{E}_3 \exp[-2\pi\,\mathrm{i}z_0/\lambda] = \vec{E}_{\mathrm{r}} \exp[\mathrm{i}(A_2 - \omega t + \varphi)]. \tag{6}$$

After transmitting through the graphene layer for the second time, i.e. from the bottom up, the electrical field of EM wave will be written as

$$\vec{E}_5 = \vec{E}_4 \exp[-A_1]\exp[\mathrm{i}A_2] = \vec{E}_{\mathrm{r}} \exp[\mathrm{i}(2A_2 - \omega t + \varphi)]\exp[-A_1]. \tag{7}$$

As a result, the power absorbed in the graphene monolayer is given by

$$\begin{aligned} P_{G,2} = A(I_4 - I_5) &= A\left(\left\langle(\mathrm{Re}E_4)^2\right\rangle_t - \left\langle(\mathrm{Re}E_5)^2\right\rangle_t\right) \\ &= (1/2)AE_{\mathrm{r}}^2(1 - \exp[-2A_1]) = (1/2)AR_{\mathrm{Si}}E_0^2 \exp[-2A_1](1 - \exp[-2A_1]) \\ &\approx 2A_1 R_{\mathrm{Si}} A I_0 = \alpha_{\mathrm{G}} a_{\mathrm{G}} A R_{\mathrm{Si}} I_0. \end{aligned} \tag{8}$$

In the above equations, we took into account that $A_1 = 2\pi\kappa a_G/\lambda \ll 1$, which leads to $\exp[-2A_1] \approx 1$ and $(1 - \exp[-2A_1]) \approx 2A_1$. The total power absorbed in graphene after EM wave passes twice through it can be now written as

$$P_G = P_{G,1} + P_{G,2} = \alpha_G a_G (1 + R_{Si}) I_o A. \tag{9}$$

Expressing I_0 through P_G we have

$$I_0 = \frac{P_G}{\alpha_G a_G (1 + R_{Si}) A}. \tag{10}$$

Plugging equation (10) to equation (1), we obtain the following equation for the integrated intensity of Raman light reflected from graphene:

$$\Delta I_G = \frac{N}{A}\sigma_G \frac{P_G}{\alpha_G a_G (1 + R_{Si})}. \tag{11}$$

Let us now consider the light absorption and Raman scattering in bulk graphite. The highly oriented crystalline graphite consists of atomic planes of graphene, which are bound by the weak Van der Waals interaction. For light with energy above 0.5 eV graphite behaves essentially as a collection of independent graphene layers [20]. It is also confirmed by the results of measurements of the light absorption in graphene multilayers, which proved that for a wide range of wavelengths the absorption is constant per atomic layer [18, 19]. In our analysis, we take into account that the absorption coefficient and Raman scattering cross-section defined per layer are the same for graphene and for the single atomic plane in bulk graphite. The electric field intensity created by the incident EM wave in nth atomic layer is $\vec{E}(n) = \vec{E}_0 \exp[2\pi i(n_0 + i\kappa_B)na_B/\lambda - i\omega t]$, where a_B is the distance between atomic planes in bulk graphite. After the Raman scattering event the intensity in the scattered wave will be given by $\vec{E}^R = \vec{E}_0^R \exp[2\pi i(n_0 + i\kappa_B)na_B/\lambda] \exp[2\pi i(n_0 + i\kappa_B)na_B/\lambda - i\omega t + 2\pi i\delta_n]$, where $\delta_n(t)$ is the phase, which appears after absorption or emission of a phonon. This phase is a random function of time varying from photon to photon. Summing the electric field intensities of the Raman scattered waves one can obtain the following:

$$\vec{E}^R_{tot} = \sum_n \vec{E}_0^R \exp[4\pi i(n_0 + i\kappa_B)na_B/\lambda - i\omega t] \exp[2\pi\, i\delta_n], \quad \text{and}$$

$$(\mathrm{Re}\vec{E}^R_{tot})^2 = \sum_{n,n'} (\vec{E}_0^R)^2 \exp[-4\pi\kappa_B(n + n')a_B] \cos(4\pi n_0 n a_B/\lambda - \omega t + 2\pi\delta_n) \times \cos(4\pi n_0 n' a_B/\lambda - \omega t + 2\pi\delta_{n'}). \tag{12}$$

In order to average over the random phases we recall that the cosines' values are between -1 and $+1$ with the average for the random variables being equal to zero for $n \neq n'$. Therefore, one can write the following expression:

$$\left\langle (\mathrm{Re}\vec{E}^R_{tot})^2 \right\rangle_\delta = \sum_n (\vec{E}_0^R)^2 \exp[-8\pi\kappa_B n a_B] \cos^2(4\pi n_0 n a_B/\lambda - \omega t + 2\pi\delta_n). \tag{13}$$

Averaging over the whole time period, we obtain for the phase factor

$$\left\langle \cos^2(4\pi n_0 n a_B/\lambda + 2\pi\delta_n - \omega t) \right\rangle_t = \int_0^{2\pi} \cos^2\varphi\, d\varphi = 1/2. \tag{14}$$

As a result, for the intensity of the Raman scattered light from the stack of atomic planes, we can write

$$I^{\mathrm{R}} = \frac{1}{2}\sigma_{\mathrm{B}} E_0^2 \sum_{n=1}^{\infty} \exp[-8\pi\kappa_{\mathrm{B}} n a_{\mathrm{B}}/\lambda] = \frac{\sigma_{\mathrm{B}} I_0}{1-\exp[-8\pi\kappa_{\mathrm{B}} a_{\mathrm{B}}/\lambda]}$$

$$= \frac{\sigma_{\mathrm{B}} I_0}{1-\exp[-2a_{\mathrm{B}}\alpha_{\mathrm{B}}]} \approx \sigma_{\mathrm{B}}/(2a_{\mathrm{B}}\alpha_{\mathrm{B}}) I_0 = (\sigma_{\mathrm{B}}/(2a_{\mathrm{B}}\alpha_{\mathrm{B}}))(P_{\mathrm{D}}/A), \tag{15}$$

where $\alpha_{\mathrm{B}} = 4\pi\kappa_{\mathrm{B}}/\lambda$. Based on the above expression, the integrated Raman scattering intensity can be written as $\Delta I_{\mathrm{B}} = N I_{\mathrm{R}} = N I_0 \sigma_{\mathrm{B}}/(2a_{\mathrm{B}}\alpha_{\mathrm{B}})$. Taking into account that a part of the incident power which is reflected from graphite and does not contribute to the Raman scattered intensity, one obtains

$$\Delta I_{\mathrm{Bulk}} = (1/2)(N/A)(\sigma_{\mathrm{B}}/\alpha_{\mathrm{B}} a_{\mathrm{B}}) P_{\mathrm{D}}(1-R_{\mathrm{B}}), \tag{16}$$

where R_{B} is the graphite reflection coefficient.

Combining equations (11) and (16) and introducing the ratio $\varsigma = \overline{\Delta I_{\mathrm{G}}}/\overline{\Delta I_{\mathrm{Bulk}}}$, which has to be determined experimentally, we obtain the final expression for the power absorbed in graphene:

$$P_{\mathrm{G}} = (\varsigma/2)[\sigma_{\mathrm{B}}\alpha_{\mathrm{G}} a_{\mathrm{G}}/\sigma_{\mathrm{G}}\alpha_{\mathrm{B}} a_{\mathrm{B}}](1+R_{\mathrm{Si}})(1-R_{\mathrm{B}}) P_{\mathrm{D}}. \tag{17}$$

The above expression allowed us to measure the heating power dissipated in the suspended portion of graphene under the specific conditions of the experiment. The ratio $\varsigma = \overline{\Delta I_{\mathrm{G}}}/\overline{\Delta I_{\mathrm{Bulk}}}$, measured for graphene and reference bulk graphite for the G peak and the same frequency interval, stays nearly constant over the excitation power range used in the experiments. The reflection coefficients for silicon and bulk graphite are tabulated quantities but can also be measured directly while P_{D} is the actual reading of the power detector taken at the position of the sample. Since the microscopic in-plane Raman cross-sections and absorption coefficients are same for graphene and bulk graphite, the square bracket term in equation (17) is close to one.

With equation (17) serving as the calibration law for converting P_{D} to P_{G}, the measurement of the thermal conductivity of suspended graphene reduces to measuring the Raman shift $\Delta\omega_G$ as a function of the heating power P_{D} determined by the detector (see figure 3). The measured slope $\Delta\omega/\Delta P_{\mathrm{D}}$, ratio of the integrated intensities ζ and the temperature coefficient χ_{G} give the value of the thermal conductivity of graphene. Initially, the thermal data extraction was accomplished using the simple 1D model, and later improved by utilizing the numeric solution of the heat diffusion equation for a given flake shape. It has been found that the thermal conductivity for the single-layer partially suspended graphene is in the range from ≈ 3000–$5300\,\mathrm{W\,mK^{-1}}$ depending on the width (lateral size) of the graphene flakes. This value is very high as compared to other carbon materials [21]–[26]. Table 1 summarizes the thermal conductivities of graphene, CNTs and bulk graphite. One can see that there is a wide data scatter for the reported values of the thermal conductivity of CNTs. The conventionally accepted values for CNTs are $K \approx 3000$–$3500\,\mathrm{W\,mK^{-1}}$. Thus, graphene can outperform CNTs as the heat conductor. Owing to its planar geometry, graphene may have potential for lateral heat spreading. It is still remains unclear as to how the thermal conductivity of graphene will be affected when graphene layer is embedded inside the device structure or how the heat conduction ability will evolve by increasing the number of atomic layers.

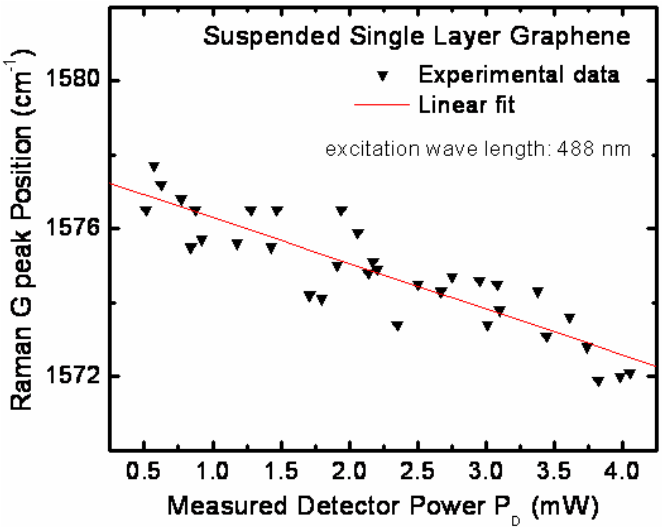

Figure 3. Raman G peak position shift with respect to the change in the heating power P_{D} on the sample surface. The heating power P_{D} is correlated with the power dissipated in graphene P_{G} through the calibration procedure.

Table 1. Experimental thermal conductivity of graphene and CNTs near RT.

Sample	K (W mK^{-1})	Method	Comments	Reference
Graphene	~3080–5300	Optical	Single layer	Balandin *et al* [3, 4]
MW-CNT	>3000	Electrical	Individual	Kim *et al* [21]
SW-CNT	~3500	Electrical	Individual	Pop *et al* [22]
SW-CNT	1750–5800	Thermocouples	Bundles	Hone *et al* [23]
SW-CNT	3000–7000	Thermocouples	Individual	Yu *et al* [24]
Graphite	~2000	Variety	In-plane (basal)	Klemens [25, 26]

4. Formal theory of the phonon heat conduction in graphene

In this section, we outline the formal theory of heat conduction in graphene. The heat flux along a graphene atomic plane can be calculated according to the expression given in [27]. Multiplied by the system volume the 'total heat flux' can be written as

$$\vec{W} = \sum_{s,\vec{q}} \vec{v}(s,\vec{q})\hbar\omega_s(\vec{q})N(\vec{q},\omega_s(\vec{q})) = \sum_{s,\vec{q}} \vec{v}(s,\vec{q})\hbar\omega_s(\vec{q})n(\vec{q},\omega_s), \tag{18}$$

where $\vec{v}(s,\vec{q})\hbar\omega_s(\vec{q})$ is the energy carried by one phonon, $\vec{v}(s,\vec{q}) = \mathrm{d}\omega_s/\mathrm{d}q$ is the phonon group velocity and $N(\omega,\vec{q}) = N_0(\omega,\vec{q}) + n(\omega,\vec{q})$ is the number of phonons in the flux. Here N_0 is the Bose–Einstein distribution function and $n = -\tau_{\mathrm{tot}}(\vec{v}\nabla T)\partial N_0/\partial T$ is the non-equilibrium part of the phonon distribution function N, where τ_{tot} is the total phonon relaxation time and T is the absolute temperature.

Comparing the microscopic expression

$$\vec{W} = -\sum_{\beta} (\nabla T)_\beta \sum_{s,\vec{q}} \tau_{\mathrm{tot}}(s,\vec{q})v_\beta(s,\vec{q})\frac{\partial N_0(\omega_s)}{\partial T}\vec{v}(s,\vec{q})\hbar\omega_s(\vec{q}) \tag{19}$$

with the macroscopic definition of the thermal conductivity

$$W_\alpha = -\kappa_{\alpha\beta}(\nabla T)_\beta h L_x L_y, \tag{20}$$

we obtain the following expression for the thermal conductivity tensor:

$$\kappa_{\alpha\beta} = \frac{1}{hL_xL_y}\sum_{s,\vec{q}} \tau_{\rm tot}(s,\vec{q})v_\alpha(s,\vec{q})v_\beta(s,\vec{q})\frac{\partial N_0(\omega_s)}{\partial T}\hbar\omega_s(\vec{q}). \tag{21}$$

Here $L_x = d$ is the sample width (graphene flake width), L_y is the sample length and $h = a_{\rm G} = 0.35$ nm is the thickness of graphene. The diagonal element of the thermal conductivity tensor, which corresponds to the phonon flux along the temperature gradient, is given by

$$\kappa_{\alpha\alpha} = \frac{1}{hL_xL_y}\sum_{s,\vec{q}} \tau_{\rm tot}(s,\vec{q})v^2(s,\vec{q})\cos^2\varphi\frac{\partial N_0(\omega_s)}{\partial T}\hbar\omega_s(\vec{q}). \tag{22}$$

Finally, making a transition from the summation to the integration and taking into account the 2D density of phonon states, we obtain the following expression for the scalar thermal conductivity:

$$K = \frac{1}{4\pi k_{\rm B}T^2h}\sum_s \int_0^{q_{\max}} \left\{\left[\hbar\omega_s(q)\frac{{\rm d}\omega_s(q)}{{\rm d}q}\right]^2 \tau_{\rm tot}(s,q)\frac{\exp[\hbar\omega_s(q)/kT]}{[\exp[\hbar\omega_s(q)/kT]-1]^2}q\right\}{\rm d}q. \tag{23}$$

The detailed description of the theoretical formalism for the phonon heat conduction in graphene was recently reported by some of us elsewhere [7]. Our theoretical approach utilized an original *phase-diagram technique* to account for all three-phonon Umklapp scattering channels allowed by the energy and momentum conservation. We consider two types of the three-phonon Umklapp scattering processes [27]–[29]. The first type is the scattering when a phonon with the wave vector $\vec{q}(\omega)$ absorbs another phonon from the heat flux with the wave vector $\vec{q}'(\omega')$, i.e. the phonon leaves the state $\vec{q}$. For this type of scattering processes, the momentum and energy conservation laws are written as

$$\begin{aligned} &\vec{q}+\vec{q}' = \vec{b}_i+\vec{q}'', \\ &\omega+\omega' = \omega'', \end{aligned} \tag{24}$$

where $\vec{b}_i$, $i = 1, 2, 3$, is one of the vectors of reciprocal lattice (see figure 4(a)). The processes of the second type are those that occur when the phonons $\vec{q}$ of the heat flux decay into two phonons with the wave vectors $\vec{q}'$ and $\vec{q}''$ leaving the state $\vec{q}$, or, alternatively, when two phonons $\vec{q}'(\omega')$ and $\vec{q}''(\omega'')$ merge together forming a phonon with the wave vector $\vec{q}(\omega)$, which correspond to the phonon coming to the state $\vec{q}(\omega)$. The conservation laws for this type are given by

$$\begin{aligned} &\vec{q}+\vec{b}_i = \vec{q}'+\vec{q}'', \quad i = 4, 5, 6, \\ &\omega = \omega'+\omega''. \end{aligned} \tag{25}$$

To find all the possible three-phonon processes, we used a fine mesh $q_j = (j-1)\Delta q$ ($j = 1, \ldots, 1001$) with the step $\Delta q = q_{\max}/1000 \approx 0.015\,{\rm nm}^{-1}$. For each phonon mode (q_i, s), we found all pairs of the phonon modes $(\vec{q}', s')$ and $(\vec{q}'', s'')$ such that the conditions of equations (24) and (25) are met. As a result, we constructed in $(\vec{q}')$-space the *phase diagrams* for all allowed three-phonon transitions [7]. A sample *phase diagram* is depicted in figure 4(b) for different (q_i, s) and $(\vec{q}', s')$.

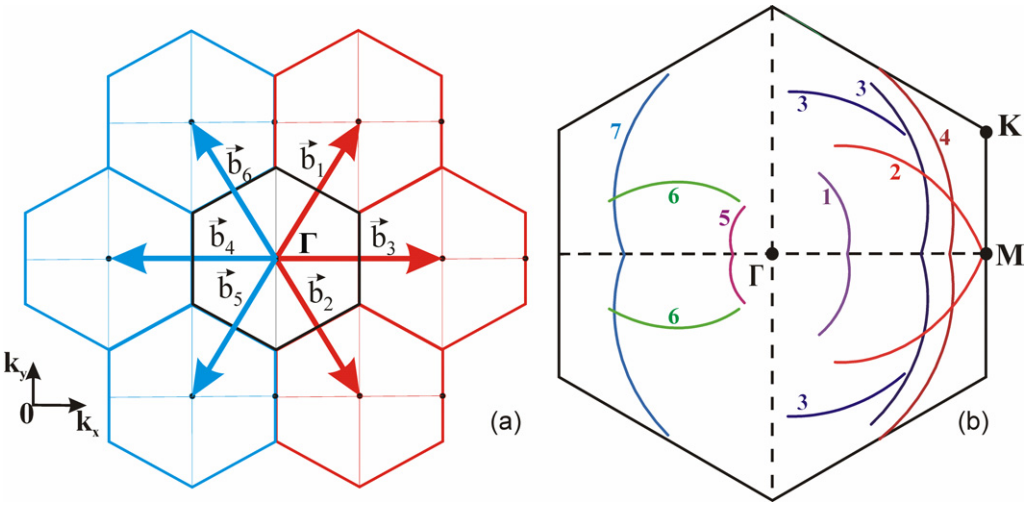

Figure 4. (a) Schematic view of 2D BZs in graphene. (b) Three-phonon scattering diagrams used for accounting of the LA and TA phonon Umklapp scattering processes with the participation of the following phonons: (i) TA + LA → TO, $q = 5.8\,\mathrm{nm}^{-1}$; (ii) LA + ZA → LA, $q = 5.8\,\mathrm{nm}^{-1}$; (iii) TA + TA → LA, $q = 5.8\,\mathrm{nm}^{-1}$; (iv) TA + TA → LA, $q = 4.4\,\mathrm{nm}^{-1}$; (v) TA → ZA + ZO, $q = 13.1\,\mathrm{nm}^{-1}$; (vi) LA → TA + TA, $q = 10.1\,\mathrm{nm}^{-1}$ and (vii) LA → ZA + ZO, $q = 10.1\,\mathrm{nm}^{-1}$.

Using the general expression for a matrix element of the three-phonon interaction [27]–[29] and taking into account all relevant phonon branches and their dispersion as well as all unit vectors of the reciprocal lattice $\vec{b}_1 \ldots \vec{b}_6$, directed from the Γ point to the centers of the neighboring unit cells (see figure 4(a)), we obtain the following for the Umklapp scattering rates:

$$\frac{1}{\tau_{\mathrm{U}}^{(\mathrm{I}),(\mathrm{II})}(s,\vec{q})} = \frac{\hbar\gamma_s^2(\vec{q})}{3\pi\rho v_s^2(\vec{q})} \sum_{s's'';\vec{b}_i} \int\int \omega_s(\vec{q})\omega'_{s'}(\vec{q}')\omega''_{s''}(\vec{q}'') \left\{ N_0[\omega'_{s'}(\vec{q}')] \mp N_0[\omega''_{s''}(\vec{q}'')] + \frac{1}{2} \mp \frac{1}{2} \right\}$$
$$\times \delta[\omega_s(\vec{q}) \pm \omega'_{s'}(\vec{q}') - \omega''_{s''}(\vec{q}'')]\, \mathrm{d}q'_l\, \mathrm{d}q'_\perp. \qquad (26)$$

Here q'_l and $q'_\perp$ are the components of the vector $\vec{q}'$ parallel or perpendicular to the lines defined by equations (24) and (25), correspondingly, $\gamma_s(\vec{q})$ is the mode-dependent Gruneisen parameter, which is determined for each phonon wave vector and polarization branch and ρ is the surface mass density. In equation (26), the upper signs correspond to the processes of the first type, whereas the lower signs correspond to those of the second type. The integrals for $q_l, q_\perp$ are taken along and are perpendicular to the curve segments, correspondingly, where the conditions of equations (24) and (25) are met (see figure 4(b)). Integrating along $q_\perp$, we obtain the line integral

$$\frac{1}{\tau_{\mathrm{U}}^{(I),(II)}(s,\vec{q})} = \frac{\hbar\gamma_s^2(\vec{q})\omega_s(\vec{q})}{3\pi\rho v_s^2(\vec{q})} \sum_{s's'';\vec{b}} \int_l \frac{\pm(\omega''_{s''} - \omega_s)\omega''_{s''}}{v_\perp(\omega'_{s'})} \left(N'_0 \mp N''_0 + \frac{1}{2} \mp \frac{1}{2} \right) \mathrm{d}q'_l. \qquad (27)$$

The integration in equation (27) is carried out along the curve segments l, as those shown in figure 4(b). The integration in the expression for the scattering rate is a nontrivial task. Previously, in the calculation of the thermal conductivity of conventional materials, it was done

rather roughly with many simplifying assumptions. Most of the authors assumed that the phonon with the wave vector $\vec{q}'$ is on the surface of the BZ so that for any $\vec{q}$, the following relation is satisfied $\vec{q}+\vec{q}'=\vec{b}+\vec{q}''$. The frequency $\omega(q')$ in the equations similar to our equation is replaced with $\omega(q')=\omega_{\mathrm{T}}$, where ω_{T} is the maximum value of the transverse acoustic phonons. Next, for each q on the BZ surface, a circle with the radius r_{C} was introduced within which (for a given q) the conditions of equations (24) and (25) are satisfied. In such an approach, the integration over $\vec{q}'$ is reduced to multiplication by the circle area πr_{C}^2. In order to capture the specifics of heat conduction in a 2D system such as graphene we avoided these simplifying assumptions, and performed the integration in equation (27) accurately. The latter was made possible via the scattering *phase diagram* technique developed by us.

As the first step, we found the points in BZ for which the condition $\omega(\vec{q})+\omega(\vec{q}')=\omega(\vec{q}'')$ is satisfied. To do this, we fixed q and numerically examined all pairs of $\vec{q}'$ and $\vec{q}''$, belonging to BZ, and selected such points in 2D reciprocal space $(\vec{q}',\ \omega_s'(\vec{q}'))$ and $(\vec{q}'',\ \omega_s''(\vec{q}''))$ where the conditions of equations (24) and (25) are valid for a given q. Such points form the curve segments in the scattering diagrams (see figure 4(b)). These curves are nothing else but the lines along which the integral in equation (27) is taken. This procedure was repeated for all phonon polarization branches and all values of $\vec{q}$. As a result, we found numerically, for all possible $\vec{q}$ and for all polarization branches TA, LA, ZA, TO, LO, ZO, the lines in BZ along which the conditions of equations (24) and (25) are valid. The integral in equation (27) was taken numerically along these lines. The contributions from the separates lines (segments in the phase diagrams shown in figure 4(b)) were summed to obtain the total Umklapp scattering rate. The outlined procedure constitutes the essence of our diagram technique.

The combined scattering rate in both types of the three-phonon Umklapp processes for a phonon in the state $(s,\vec{q})$ can be calculated as

$$\frac{1}{\tau_{\mathrm{U}}(s,\vec{q})}=\frac{1}{\tau_{\mathrm{U}}^{I}(s,\vec{q})}+\frac{1}{\tau_{\mathrm{U}}^{II}(s,\vec{q})}. \tag{28}$$

One should note here that for the small phonon wave vectors (long wavelength), $q\to 0$, the Umklapp-limited phonon life-time $\tau_{\mathrm{U}}\to\infty$. For this reason, the calculation of the intrinsic thermal conductivity with only Umklapp scattering is not possible without an arbitrary truncation procedure. To avoid the unphysical assumptions about the limits of the integration, we accurately include the phonon scattering on boundaries. In the case of graphene, the boundary scattering term correspond to scattering from the rough edges of graphene flakes. No scattering happens from the top and bottom sides of graphene flake since it is only one atomic layer thick and the phonon flux is parallel to the graphene plane. We evaluate the rough edges' scattering using the Ziman equation [30]:

$$\frac{1}{\tau_{\mathrm{B}}(s,q)}=\frac{v_s(\omega_s)}{L}\frac{1-p}{1+p}. \tag{29}$$

Here p is the specularity parameter, which depends on the roughness of the graphene edges and L is the width of the graphene flake. The total phonon relaxation rate is given by

$$\frac{1}{\tau_{\mathrm{tot}}(s,q)}=\frac{1}{\tau_{\mathrm{U}}(s,q)}+\frac{1}{\tau_{\mathrm{B}}(s,q)}. \tag{30}$$

It is important to emphasize that the thermal conductivity of the 2D system such as graphene cannot be determined without the restriction on the phonon MFP in the long wavelength limit. The phonon scattering on edges restricts the MFP in the formal theory of thermal conductivity.

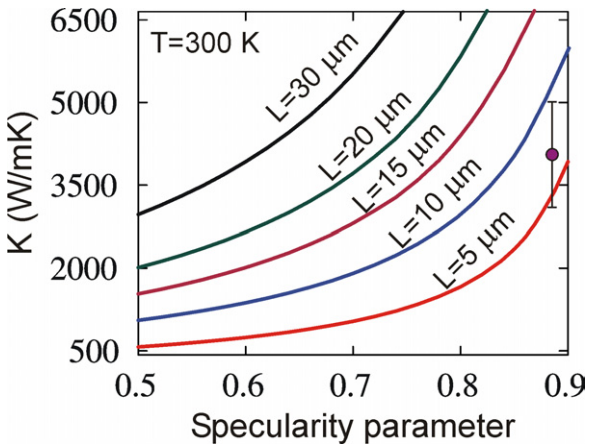

Figure 5. Calculated thermal conductivity of the suspended graphene as a function of the specularity parameter p for the phonon scattering from the flake edges. Note a strong dependence on the size of the graphene flakes.

In this sense the thermal conductivity limited by the Umklapp and boundary scattering can be considered as an *intrinsic* property of a graphene flake of a particular size. The extrinsic effects, which reduce the thermal conductivity, such as phonon scattering on defects, impurities and grain boundaries are not included into the consideration. The RT *intrinsic* thermal conductivity of graphene as a function of the specularity parameter is shown in figure 5. The specularity parameter is defined by the edge roughness: $p = 0$ corresponds to the perfectly diffusive phonon scattering from the edges while $p = 1$ corresponds to the perfectly specular scattering, which does not contribute to the thermal resistance. The results were calculated for different sizes (widths) of the graphene flakes. The experimental data point after Balandin *et al* [3, 4] is also shown for comparison.

5. Simple model of the phonon thermal conductivity of graphene

The calculation of the thermal conductivity within the formal theory outlined in the previous section is an accurate but a rather complicated procedure. In this section, we describe a simpler model of the thermal conductivity of graphene. This model originates from the Klemens' approach to the thermal conductivity analysis of bulk graphite and graphene [25, 26]. We substantially modified it by using a more general expression for the thermal conductivity, introducing two Gruneisen parameters γ_s obtained independently for each of the heat conducting phonon polarization branches s, and keeping separate the velocities and cut-off frequencies for each phonon branch. These changes allowed us to reflect the specifics of the phonon dispersion in graphene. The effective parameters γ_s are computed by averaging the phonon-mode-dependent $\gamma_s(\vec{q})$ for all relevant phonons (here $\vec{q}$ is the phonon wave vector). The phonon branches, which carry heat, are longitudinal acoustic (LA) and transverse acoustic (TA). The out-of-plane transverse acoustic phonons (ZA) do not make contributions to heat conduction due to their low group velocity and high $\gamma_s(\vec{q})$. There is a clear difference in the heat transport in basal planes of bulk graphite and in single-layer graphene [25, 26]. In the former, the heat transport is approximately 2D only till some low-bound cut-off frequency

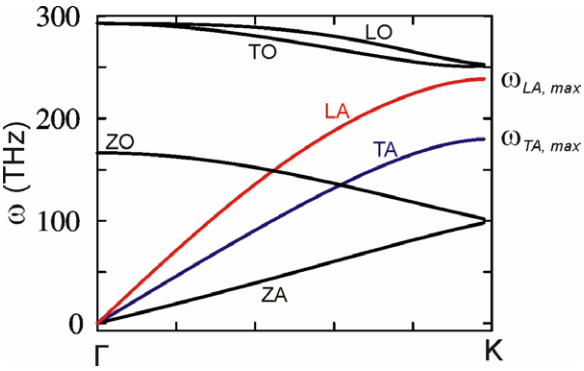

Figure 6. Phonon energy spectra in graphene calculated by using the VFF method.

ω_C. Below ω_C there appears strong coupling with the cross-plane phonon modes and heat starts to propagate in all directions, which reduces the contributions of these low-energy modes to heat transport along basal planes to negligible values. In bulk graphite, there is a physically reasonable reference point for the onset of the cross-plane coupling, which is the ZO′ phonon branch near ~4 THz observed in the spectrum of bulk graphite. The presence of ZO′ branch and corresponding ω_C allows one to avoid the logarithmic divergence in the Umklapp-limited thermal conductivity integral and calculate it without considering other scattering mechanisms.

The physics of heat conduction is principally different in graphene where the phonon transport is purely 2D all the way to zero-phonon frequency $\omega(q = 0) = 0$. There is no onset of the cross-plane heat transport at the long-wavelength limit in the system, which consists of only one atomic plane. There is no ZO′ branch in the phonon dispersion of graphene (see figure 6). Thus, the cut-off frequency for Umklapp processes cannot be introduced by analogy with bulk graphite. Using an expression for the three-phonon Umklapp scattering from [25, 26] but introducing separate lifetimes for LA and TA phonons, we have

$$\tau^K_{U,s} = \frac{1}{\gamma_s^2}\frac{M\upsilon_s^2}{k_B T}\frac{\omega_{s,\max}}{\omega^2}, \tag{31}$$

where $s =$ TA or LA, υ_s is the average phonon velocity for a given branch, T is the absolute temperature, k_B is the Boltzmann constant, $\omega_{s,\max}$ is the maximum cut-off frequency for a given branch and M is the mass of the unit cell. To determine γ_s, we averaged $\gamma_s(q)$ obtained from the accurate phonon dispersion calculated by using the VFF method [7] and the *ab initio* theory [31]. Substituting $\tau_{tot} = \tau^K_{U,s}$ in equation (23), one can obtain the following formula for intrinsic thermal conductivity in graphene:

$$K_U = \frac{1}{4\pi k_B T^2 h}\sum_{s=TA,LA}\int_{q_{min}}^{q_{max}}\left\{\left[\hbar\omega_s(q)\frac{d\omega_s(q)}{dq}\right]^{-2}\tau^K_{U,s}(q)\frac{\exp[\hbar\omega_s(q)/kT]}{[\exp[\hbar\omega_s(q)/kT]-1]^2}q\right\}dq. \tag{32}$$

The above equation can be used to calculate the thermal conductivity with the actual dependence of the phonon frequency $\omega_s(q)$ and the phonon velocity $d\omega_s(q)/dq$ on the phonon wavenumber. To simplify the model, we can use the liner dispersion $\omega_s(q) = \upsilon_s q$ and rewrite it as

$$K_U = \frac{\hbar^2}{4\pi k_B T^2 h}\sum_{s=TA,LA}\int_{\omega_{min}}^{\omega_{max}}\left\{\omega^3\tau^K_{U,s}(\omega)\frac{\exp[\hbar\omega/kT]}{[\exp[\hbar\omega/kT]-1]^2}\right\}d\omega. \tag{33}$$

Substituting equation (31) into equation (33) and performing integration we obtain

$$K_{\mathrm{U}} = \frac{M}{4\pi T h} \sum_{s=\mathrm{TA,LA}} \frac{\omega_{s,\max} \upsilon_s^2}{\gamma_s^2} F(\omega_{s,\min}, \omega_{s,\max}), \tag{34}$$

where

$$\begin{aligned} F(\omega_{s,\min}, \omega_{s,\max}) &= \int_{\hbar\omega_{s,\min}/k_{\mathrm{B}}T}^{\hbar\omega_{s,\max}/k_{\mathrm{B}}T} \xi \frac{\exp(\xi)}{[\exp(\xi)-1]^2} \mathrm{d}\xi \\ &= \left[\ln\{\exp(\xi)-1\} + \frac{\xi}{1-\exp(\xi)} - \xi \right] \Bigg|_{\hbar\omega_{s,\min}/k_{\mathrm{B}}T}^{\hbar\omega_{s,\max}/k_{\mathrm{B}}T}. \end{aligned} \tag{35}$$

In the above equation, $\xi = \hbar\omega/k_{\mathrm{B}}T$, and the upper cut-off frequencies $\omega_{s,\max}$ are defined from the actual phonon dispersion in graphene, calculated by using the VFF model [7] and presented in figure 6: $\omega_{\mathrm{LA,max}} = 241$ THz, $\omega_{\mathrm{LA,max}} = 180$ THz. The low-bound cut-off frequencies $\omega_{s,\min}$ for each s are determined from the condition that the phonon MFP cannot exceed the physical size L of the flake, given as

$$\omega_{s,\min} = \frac{\upsilon_s}{\gamma_s} \sqrt{\frac{M\upsilon_s}{k_{\mathrm{B}}T} \frac{\omega_{s,\max}}{L}}. \tag{36}$$

The integrand in equation (35) can be further simplified near RT when $\hbar\omega_{s,\max} > k_B T$, and it can be expressed as

$$F(\omega_{s,\min}) \approx -\ln\{|\exp(\hbar\omega_{s,\min}/k_{\mathrm{B}}T) - 1|\} + \frac{\hbar\omega_{s,\min}}{k_{\mathrm{B}}T} \frac{\exp(\hbar\omega_{s,\min}/k_{\mathrm{B}}T)}{\exp(\hbar\omega_{s,\min}/k_{\mathrm{B}}T) - 1}. \tag{37}$$

The obtained equations (34) and (37) constitute a simple analytical model for calculation of the thermal conductivity of the graphene layer, which retains such important features of graphene phonon spectra as different υ_s and γ_s for LA and TA branches. The model also reflects the 2D nature of heat transport in graphene all the way down to zero-phonon frequency. Our equation (31) reduces to Klemens' formula for graphene [26] in the limit $\xi \to 0$ ($\hbar\omega \ll k_{\mathrm{B}}T$) and additional assumption of the same γ_s and υ_s for LA and TA phonons.

Using equations (32) and (34)–(37) of the simple model we calculated the Umklapp-limited *intrinsic* thermal conductivity of graphene as a function of temperature. The results are shown in figure 7 for two different widths of graphene flakes. The Gruneisen parameters used in this calculation, $\gamma_{\mathrm{LA}} = 1.8$ and $\gamma_{\mathrm{TA}} = 0.75$, were obtained by averaging of $\gamma_s(q)$ [32]. The thermal conductivity calculated with the exact $\omega_s(q)$ and the phonon velocity $\mathrm{d}\omega_s(q)/\mathrm{d}q$ (shown by the dashed curves) is slightly smaller (by 5–10%) than those obtained with the simplified equations (34)–(37) due to the decrease of $\mathrm{d}\omega_s(q)/\mathrm{d}q$ with increasing q. The difference between thermal conductivities increases with increasing temperature as the condition $\hbar\omega_{s,\max} > k_{\mathrm{B}}T$ breaks down. One should note a very different temperature dependence obtained within this model for the relatively small graphene flakes (10 μm) as compared to that for large flakes (100 μm). In the very narrow graphene flakes and nanoribbons, the thermal conductivity increases with temperature, which is related to the size (edge) effect on the phonon MFP.

In figure 8, we present the calculated RT thermal conductivity as a function of the flake width. The dashed curves are obtained using equation (23) with the total relaxation rate $1/\tau_{\mathrm{tot}}(s,q) = 1/\tau^K_{\mathrm{U},s}(\omega_s(q)) + 1/\tau_{\mathrm{B}}(s,q)$, explicitly taking into account the phonon scattering on graphene edges. The solid curve is obtained from the simplified approach (equations (31)–(37))

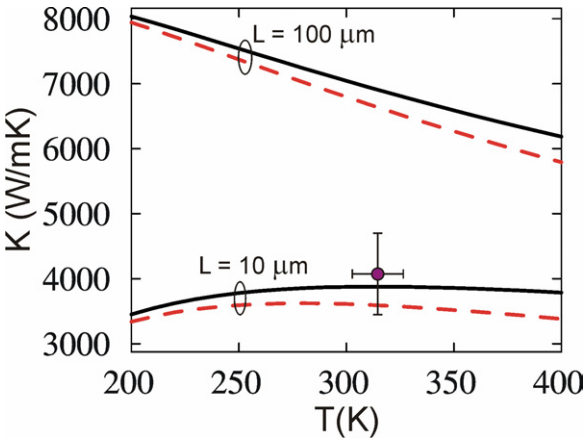

Figure 7. Calculated thermal conductivity of graphene as a function of temperature for two distinctively different flake sizes. An experimental data point after Balandin *et al* [3, 4] is also shown for comparison.

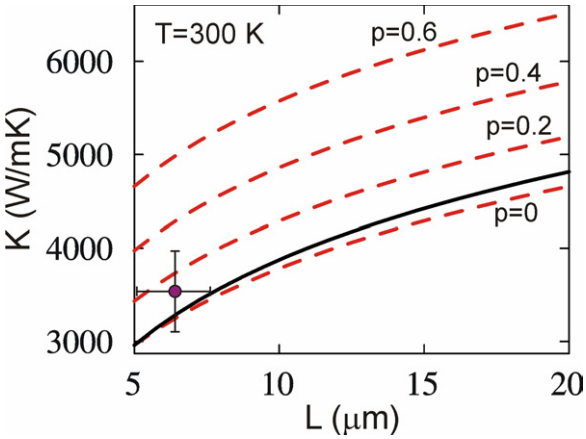

Figure 8. Calculated RT thermal conductivity of graphene as a function of the lateral size for several values of the specularity parameter p. An experimental data point after Balandin *et al* [3, 4] is also shown for comparison.

in which the edge scattering is not directly included. Instead, the phonon MFP is limited by the physical size of the flake. The dashed curves are plotted for different values of the specularity parameter p. Using both approaches we obtained similar dependences: the *intrinsic* thermal conductivity of graphene grows with the increasing linear size of the graphene flake L. This is a manifestation of the two-dimensional nature of the phonon transport in graphene. In real experimental conductions, the thermal conductivity will also be limited by extrinsic factors (defects, impurities, grain size, etc), which prevent the growth of the thermal conductivity for very large flakes. With the decreasing specularity parameter p (more diffuse scattering), the thermal conductivity calculated with the boundary scattering term approaches the result obtained with the simple model. This is because in the simple model we neglect phonons with frequency $\omega < \omega_{\min,s}$ by completely restricting the phonon MFP to the lateral sizes of the flake. The latter corresponds to the perfectly diffusive scattering case ($p = 0$).

The described models are in good agreement with the measurements and shed light on the heat conduction properties of graphene. It also helps to understand the extremely large range of the thermal conductivity values in carbon materials, which vary from some of the lowest in amorphous carbon, nanocrystalline diamond and diamond-like carbon [33]–[36] to the highest in graphene and CNTs (see table 1). The simple model can be readily incorporated into the simulation software for the analysis of heat conduction in graphene layers and graphene devices [37, 38]. The superior thermal conductivity of graphene is beneficial for all of its proposed device applications, e.g. in low-noise transistors, sensors and interconnects [39, 40]. The application of graphene or few-layer graphene for lateral heat spreading would require special heat sinks and graphene's integration with suitable electrical insulators, e.g. synthetic diamonds. The thermal conductivity of graphene embedded within SiO_2 layers can be reduced due to the interface effects. It also decreases with the temperature due to stronger Umklapp scattering at elevated temperature [41]. A recent study of energy dissipation in graphene field-effect transistors [41] revealed the temperature dependence of the thermal conductivity of graphene in line with our theoretical prediction [7]. One should note however that our measurements were performed for partially suspended graphene with lateral heat sinks while the study reported in [41] is for graphene on SiO_2 and heat sinks at the substrate bottom, which lead to a different heat front and its dissipation through the oxide layer.

6. Conclusions

We reviewed the results of our experimental investigation of heat conduction in suspended graphene and presented their detailed theoretical interpretation. We explain the enhanced thermal conductivity of graphene as compared to that of bulk graphite basal planes by the 2D nature of heat conduction in graphene over the whole range of phonon frequencies. The intrinsic Umklapp-limited thermal conductivity of graphene grows with the increasing linear dimensions of graphene flakes and can exceed that of bulk graphite when the flake size is on the order of few micrometers. Superior thermal properties of graphene are beneficial for all proposed graphene device applications.

Acknowledgments

The work at UCR was supported, in part, by DARPA—SRC through the FCRP Center on Functional Engineered Nano Architectonics (FENA), Interconnect Focus Center (IFC) and AFOSR project on nanoscale phonon engineering. DLN and EPP acknowledge financial support from the Republic of Moldova (projects 18/ind and 06.408.036F).

References

[1] Novoselov K S, Geim A K, Morozov S V, Jiang D, Zhang Y, Dubonos S V, Grigorieva I V and Firsov A A 2004 *Science* **306** 666
Novoselov K S, Geim A K, Morozov S V, Jiang D, Katsnelson M I, Grigorieva I V, Dubonos S V and Firsov A A 2005 *Nature* **438** 197
Geim A K and Novoselov K S 2007 *Nat. Mater.* **6** 183
[2] Zhang Y B, Tan Y W, Stormer H L and Kim P 2005 *Nature* **438** 201
[3] Balandin A A, Ghosh S, Bao W, Calizo I, Teweldebrhan D, Miao F and Lau C N 2008 *Nano Lett.* **8** 902

[4] Ghosh S, Calizo I, Teweldebrhan D, Pokatilov E P, Nika D L, Balandin A A, Bao W, Miao F and Lau C N 2008 *Appl. Phys. Lett.* **92** 151911
[5] Calizo I, Miao F, Bao W, Lau C N and Balandin A A 2007 *Appl. Phys. Lett.* **91** 071913
[6] Calizo I, Balandin A A, Bao W, Miao F and Lau C N 2007 *Nano Lett.* **7** 2645
[7] Nika D L, Pokatilov E P, Askerov A S and Balandin A A 2009 *Phys. Rev.* B **79** 155413
[8] Jiang J W, Wang J S and Li B 2009 arXiv:0902.1836v1
[9] Lan J, Wang J-S, Gan C K and Chin S K 2009 *Phys. Rev.* B **79** 115401
[10] Ferrari A C *et al* 2006 *Phys. Rev. Lett.* **97** 187401
[11] Calizo I, Bao W, Miao F, Lau C N and Balandin A A 2007 *Appl. Phys. Lett.* **91** 201904
Calizo I, Teweldebrhan D, Bao W, Miao F, Lau C N and Balandin A A 2008 *J. Phys. C: Solid State Phys.* **109** 012008
[12] Wang Y Y, Ni Z H, Shen Z X, Wang H M and Wu Y H *Appl. Phys. Lett.* **92** 043121
[13] Parvizi F, Teweldebrhan D, Ghosh S, Calizo I, Balandin A A, Zhu H and Abbaschian R 2008 *Micro Nano Lett.* **3** 29
[14] Dawlaty J M, Shivaraman S, Chandrashekhar M, Rana F and Spencer M G 2008 *Appl. Phys. Lett.* **92** 042116
[15] Sun D, Wu Z-K, Divin C, Li X, Berger C, de Heer W A, First P N and Norris T B 2008 *Phys. Rev. Lett.* **101** 157402
[16] Bolotin K I, Sikes K J, Hone J, Stormer H L and Kim P 2008 *Phys. Rev. Lett.* **101** 096802
[17] Krauss B, Lohmann T, Chae D-H, Haluska M, Klitzing K-V and Smet J H 2009 *Phys. Rev.* B **79** 165428
[18] Nair R R, Blake P, Grigorenko A N, Novoselov K S, Booth T J, Stauber T, Peres N M R and Geim A K 2008 *Science* **320** 1308
[19] Kim K S, Zhao Y, Jang H, Lee S Y, Kim J M, Kim K S, Ahn J-H, Kim P, Choi J-Y and Hong B H 2009 *Nature* **457** 706
[20] Mak K F, Sfeir M Y, Wu Y, Lui C H, Misewich J A and Heinz T F 2008 *Phys. Rev. Lett.* **101** 196405
[21] Kim P, Shi L, Majumdar A and McEuen P L 2001 *Phys. Rev. Lett.* **87** 215502
[22] Pop E, Mann D, Wang Q, Goodson K and Dai H 2006 *Nano Lett.* **6** 96
[23] Hone J, Whitney M, Piskoti C and Zett A 1999 *Phys. Rev.* B **59** R2514
[24] Yu C H, Shi L, Yao Z, Li D Y and Majumdar A 2005 *Nano Lett.* **5** 1842
[25] Klemens P G 2000 *J. Wide Bandgap Mater.* **7** 332
[26] Klemens P G 2001 *Int. J. Thermophys.* **22** 265
[27] Srivastava G P 1990 *The Physics of Phonons* (Philadelphia: Institute of Physics) p 99
Bhandari C M and Rowe D M 1988 *Thermal Conduction in Semiconductors* (New York: Wiley)
[28] Klemens P G 1958 *Solid State Physics* vol 7 ed F Seitz and D Turnbull (New York: Academic) p 1
[29] Han Y-J and Klemens P G 1993 *Phys. Rev.* B **48** 6033
[30] Ziman J M 2001 *Electrons and Phonons* (Oxford: Clarendon) p 463
[31] Mounet N and Marzari N 2005 *Phys. Rev.* B **71** 205214
[32] Nika D L, Ghosh S, Pokatilov E P and Balandin A A 2009 *Appl. Phys. Lett.* **94** 203103
[33] Shamsa M, Liu W L, Balandin A A, Casiraghi C, Milne W I and Ferrari A C 2006 *Appl. Phys. Lett.* **89** 161921
[34] Liu W L, Shamsa M, Calizo I, Balandin A A, Ralchenko V, Popovich A and Saveliev A 2006 *Appl. Phys. Lett.* **89** 171915
[35] Balandin A A, Shamsa M, Liu W L, Casiraghi C and Ferrari A C 2008 *Appl. Phys. Lett.* **93** 043115
[36] Shamsa M, Ghosh S, Calizo I, Ralchenko V, Popovich A and Balandin A A 2008 *J. Appl. Phys.* **103** 083538
[37] Subrina S and Kotchetkov D 2008 *J. Nanoelectron. Optoelectron.* **3** 249
[38] Ko G and Kim J 2009 *Electrochem. Solid State Lett.* **12** H29
[39] Shao Q, Liu G, Teweldebrhan D, Balandin A A, Rumyantsev S, Shur M and Yan D 2009 *IEEE Electron Device Lett.* **30** 288
[40] Shao Q, Liu G, Teweldebrhan D and Balandin A A 2008 *Appl. Phys. Lett.* **92** 202108
[41] Freitag M, Steiner M, Martin Y, Perebeinos V, Chen Z, Tsang J C and Avouris P 2009 *Nano Lett.* **9** 1883